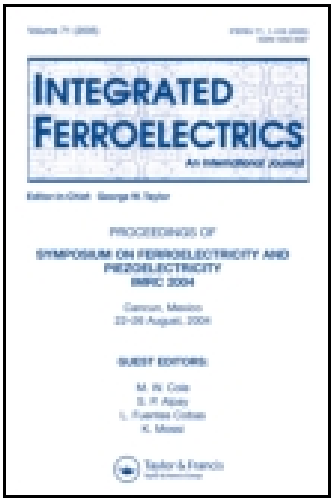

Integrated Ferroelectrics: An International Journal
Publication details, including instructions for authors and subscription information:
http://www.tandfonline.com/loi/ginf20

Ferroelectric Based Photonic Crystal Cavity by Liquid Crystal Infiltration

Filiz Karaomerlioglu[ac], Sevket Simsek[b], Amirullah M. Mamedov[c] & Ekmel Ozbay[c]

[a] Department of Electrical and Electronics Engineering, Mersin University, Mersin, Turkey

[b] Department of Materials Science and Engineering, Hakkari University, Hakkari, Turkey

[c] Nanotechnology Research Center (NANOTAM), Bilkent University, Ankara, Turkey

Published online: 26 Feb 2015.

To cite this article: Filiz Karaomerlioglu, Sevket Simsek, Amirullah M. Mamedov & Ekmel Ozbay (2014) Ferroelectric Based Photonic Crystal Cavity by Liquid Crystal Infiltration, Integrated Ferroelectrics: An International Journal, 158:1, 1-12, DOI: 10.1080/10584587.2014.956574

To link to this article: http://dx.doi.org/10.1080/10584587.2014.956574

Integrated Ferroelectrics, 158:1–12, 2014

ISSN: 1058-4587 print / 1607-8489 online
DOI: 10.1080/10584587.2014.956574

Taylor & Francis
Taylor & Francis Group

Ferroelectric Based Photonic Crystal Cavity by Liquid Crystal Infiltration

FILIZ KARAOMERLIOGLU,[1,3,*] SEVKET SIMSEK,[2] AMIRULLAH M. MAMEDOV,[3] AND EKMEL OZBAY[3]

[1]Department of Electrical and Electronics Engineering, Mersin University, Mersin, Turkey
[2]Department of Materials Science and Engineering, Hakkari University, Hakkari, Turkey
[3]Nanotechnology Research Center (NANOTAM), Bilkent University, Ankara, Turkey

A novel type of two-dimensional photonic crystal is investigated for it optical properties as a core-shell-type ferroelectric nanorod infiltrated with nematic liquid crystals. Using the plane wave expansion method and finite-difference time-domain method, the photonic crystal structure, which is composed of a photonic crystal in a core-shell-type ferroelectric nanorod, is designed for the square lattice and the hexagonal lattice. It has been used 5CB as a photonic crystal core, and $LiNbO_3$ as a ferroelectric material. The photonic crystal with a core-shell-type $LiNbO_3$ nanorod infiltrated with nematic liquid crystals is compared with the photonic crystal with solid $LiNbO_3$ rods and the photonic crystal with hollow $LiNbO_3$ rods.

Keywords Ferroelectric; photonic crystal; liquid crystal; $LiNbO_3$

1. Introduction

Progress in solid-state physics, optics of spatially structures, and nanotechnologies based on a variety of physical and chemical processes has strongly stimulated and motivated the investigation into the properties of photonic crystals (PCs) and resulted in the growth of applications of photonic band gap (PBG) materials, i.e. artificially structured materials where optical parameters are periodically modulated in space with a period of a unit PC cell on the order of the optical wavelength. Previous studies about PBG structures, PBG materials, and PCs were important investigations [1–3]. The basic feature of PCs is the presence of permitted and forbidden frequency bands of light. It is possible to manipulate the light with PCs. Due to this property, PCs hold a great potential for designing new optical devices. There has been an increase in research on tuning the optical properties of PBG to design devices. For instance, Photonic Crystal Fibers have appeared as a new class of optical waveguides. Larsen et al. describe a thermo-optic fiber switch and tunable PBGs using the thermo-optic tuning of the LC [4]. Some tunable PBG research has been done

Received in final form November 1, 2013.
*Corresponding author. E-mail: filizkrm@mersin.edu.tr
Color versions of one or more of the figures in the article can be found online at www.tandfonline.com/ginf.

in one-dimensional (1D) [5], two-dimensional (2D) [6–25], and three-dimensional (3D) [26–29] PCs.

Recently, new investigations have reached a new point of view of LCs because of the tunable light wave propagation. LCs refractive indices can be changed by rotating the directors of LCs. Liu investigated the tunable light wave propagation in two-dimensional hole-type photonic crystals infiltrated with nematic liquid crystal and the tunable absolute band gap in two-dimensional anisotropic photonic crystal structures modulated by a nematic liquid crystal [30, 31]. Liu and Chen proposed the tunable field-sensitive polarizer using hybrid conventional waveguides and PC structures with nematic liquid crystals, the tunable PC waveguide coupler with nematic liquid crystals, the tunable PC waveguide Mach–Zehnder interferometer based on nematic liquid crystals, the tunable full band gap in a three-dimensional PC structure modulated by a nematic liquid crystal, the tunable channel drop filter in a two-dimensional photonic crystal modulated by a nematic liquid crystal and the tunable band gap in a photonic crystal modulated by a nematic liquid crystal [32–37]. Liu et al. created the tunable bandgap in three-dimensional anisotropic photonic crystal structures modulated by a nematic liquid crystal and an efficient tunable negative refraction photonic crystal achieved by an elliptic rod lattice with a nematic liquid crystal [38–39].

In the present paper, we theoretically demonstrated and developed the optical properties in the 2D PC structure of a core-shell-type ferroelectric nanorod infiltrated with nematic LCs. PC structure and PC materials were especially selected wherein the optical properties are changed by an external effect such as an electric field, magnetic field, light, temperature, etc. The investigation was achieved by controlling the intensity of the optical properties that had different materials added to a certain structure.

2. Calculation Method

The fundamentals of the plane wave expansion (PWE) method and finite- difference time-domain (FDTD) method are based on a direct numerical solution of the time-dependent Maxwell's equations as illustrated in some articles [40–42]. Generally, LCs possess two kinds of dielectric constants. One is ordinary dielectric constants ε_o and the other is extraordinary dielectric constants ε_e. Light waves with electric fields perpendicular and parallel to the director of the LC have ordinary and extraordinary refractive indices, respectively. The components of the dielectric tensor of the nematic LC are represented as [43]

$$\varepsilon_{xx}(\vec{r}) = n_o^2 + \left(n_e^2 - n_o^2\right)\cos^2\theta\cos^2\emptyset \tag{1}$$

$$\varepsilon_{xy}(\vec{r}) = \varepsilon_{yx}(\vec{r}) = \left(n_e^2 - n_o^2\right)\cos^2\theta\sin\emptyset\cos\emptyset \tag{2}$$

$$\varepsilon_{xz}(\vec{r}) = \varepsilon_{zx}(\vec{r}) = \left(n_e^2 - n_o^2\right)\sin\theta\cos\theta\cos\emptyset \tag{3}$$

$$\varepsilon_{yy}(\vec{r}) = n_o^2 + \left(n_e^2 - n_o^2\right)\cos^2\theta\sin^2\emptyset \tag{4}$$

$$\varepsilon_{yz}(\vec{r}) = \varepsilon_{zy}(\vec{r}) = \left(n_e^2 - n_o^2\right)\sin\theta\cos\theta\sin\emptyset \tag{5}$$

$$\varepsilon_{zz}(\vec{r}) = n_o^2 + \left(n_e^2 - n_o^2\right)\sin^2\theta \tag{6}$$

where θ is the tilt angle of the LC director (i.e. the angle between the LC director and the XY-plane) and $\emptyset$ is the rotation angle between the projection of the LC director on the XY-plane and the X-axis, and $\vec{n}$ is the director of the LC.

On the other hand, Bloch's theorem [44] is used to expand the $H(\vec{r})$ field in terms of plane waves since the light waves are transmitted in periodic structures, as

$$H(\vec{r}) = \sum_{\vec{G}} h\left(\vec{G}\right) \hat{e}_{\vec{G}} e^{i\left(\vec{k}+\vec{G}\right)\vec{r}} \tag{7}$$

where $\vec{k}$ is a wave vector in the Brillouin zone of the lattice and $\hat{e}_{\vec{G}}$ is the direction which is perpendicular to the wave vector $\left(\vec{k}+\vec{G}\right)$ owing to the transverse character of the magnetic field $H(\vec{r})$, $\nabla \cdot H(\vec{r}) = 0$.

3. Numerical Results

The PBG is manipulated by the rotating directors of LCs under the impact of an applied electric field. Maxwell's equations, for the propagation of electromagnetic waves in a periodic arrangement of PC with nematic LCs, were solved. Using the PWE method and the FDTD method, the PC structure, composed of a PC in a core-shell-type ferroelectric nanorod infiltrated with nematic LCs, was designed for the square lattice and the hexagonal lattice. PCs structures that are designed as round rods and square rods with different lattice shape were computed. $LiNbO_3$ was used as ferroelectric material and is 5CB (4-pentyl-4′-cyanobiphenyl) as nematic LCs. The results of PC with the core-shell-type $LiNbO_3$ nanorod infiltrated with nematic LCs is compared with the PC with solid $LiNbO_3$ rods and the PC with hollow $LiNbO_3$ rods.

3.1. 2D PC of a Core-Shell-Type Ferroelectric Round Nanorod with Nematic LCs

The 2D PC structure is composed of anisotropic nematic LCs in a core-shell-type $LiNbO_3$ round nanorod with the lattice constant $a = 1\mu m$. The core-shell-type $LiNbO_3$ round nanorods are simulated in a square lattice and a hexagonal lattice. For each lattice shape, $LiNbO_3$ round nanorods, core-shell-type $LiNbO_3$ round nanorods, and core-shell-type $LiNbO_3$ round nanorods of nematic LC-infill in an air background ($\varepsilon_a = 1$) were designed. 5CB type LCs have two different principle refractive indices as an ordinary-refractive index $n_o = 1.548$ and extraordinary refractive index $n_e = 1.742$. The ordinary-refractive index of the $LiNbO_3$ nanorod is $n_o = 2.237$.

3.1.1. Square Lattice. The schematic views of the proposed 2D PC of $LiNbO_3$ round nanorods, core-shell-type $LiNbO_3$ round nanorods, and core-shell-type $LiNbO_3$ round nanorods of nematic LC-infill in an air background in a square lattice are shown in Fig. 1. The photonic band structure for TE and TM mode is calculated along with the high symmetry point for the Brillouin zone in a square lattice. Supposing the radius of the cylinders, $r = 0.3a$, the photonic band structure of the PC with $LiNbO_3$ round nanorods for a square lattice in an air background is simulated (Fig. 1(a)). There is no band gap for TE mode but we can see a two band gap of TM mode in Fig. 2(a). Their relative widths are 13.08% and 5.26%, and the center normalized frequencies are $0.376(2\pi\,\mathrm{c/a})$, and $0.632(2\pi\,\mathrm{c/a})$.

It is assumed that $r_1 = 0.3a$ and $r_2 = 0.2a$ denote the outer and inner radius of core-shell-type $LiNbO_3$ round nanorods in an air background in Fig. 1(b). Figure 2(b) shows that PBG is decreased one band gap in TM mode when the PC structure becomes core-shell-type

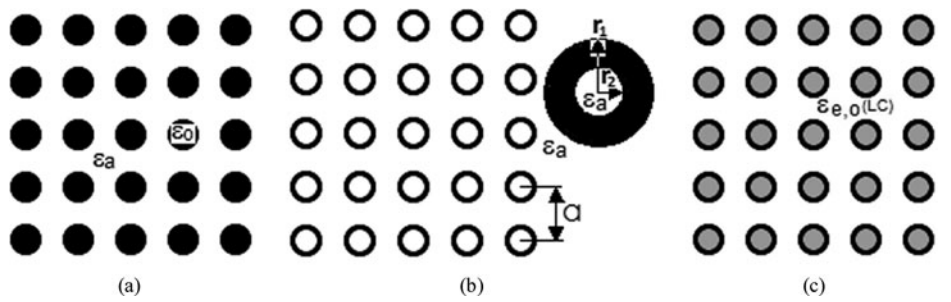

Figure 1. 2D PC structure for a square lattice (a) $LiNbO_3$ round nanorods, (b) core-shell-type $LiNbO_3$ round nanorods, and (c) core-shell-type $LiNbO_3$ round nanorods of nematic LC-infiltrated in an air background.

$LiNbO_3$ round nanorods in the air background. Its relative width is 1.13%, and its center normalized frequency is $1.102(2\pi c/a)$. The core-shell-type $LiNbO_3$ round nanorods that have been infiltrated with nematic LC are shown in Fig. 1(c). The photonic band structure of TE and TM mode is investigated for ordinary-refractive index and extraordinary refractive index, respectively. One band gap in TM mode for the extraordinary refractive index of nematic LC is shown in Fig. 3(a). The band gap has a relative width of 3.32%, and center normalized frequency of $0.405(2\pi c/a)$. As the results obtained for the ordinary-refractive index and extraordinary refractive index of nematic LC are different, it is an indication of anisotropy. By using the anisotropic features of LCs different results for TE and TM mode were obtained. This means that either the structure is rotated into a certain direction or it is infiltrated with different directivity LCs into the structure in order to be able to change the features of these structures.

It is well known that an anisotropic nanostructuring photonic band structure array is capable of changing the polarization state of transmitted or reflected light. Therefore, we also calculated the optical response of the photonic band structure for the different directivity LCs of the polarization ellipse and ellipticity of the light transmitted through photonic band array. The numerical results of the variation of full transmission by changing the direction of LC for the PC structure are presented. The transmission spectrum as a function of the frequency is computed for the ordinary-refractive index and extraordinary

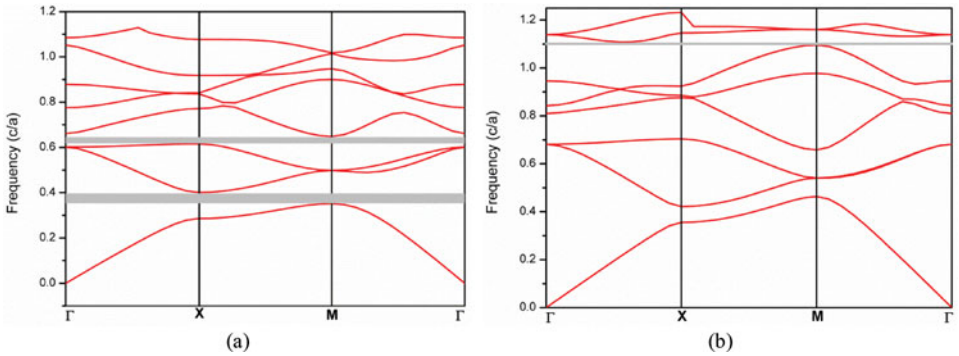

Figure 2. The photonic band structure of TM mode in a square lattice for (a) $LiNbO_3$ round nanorods, (b) core-shell-type $LiNbO_3$ round nanorods in an air background.

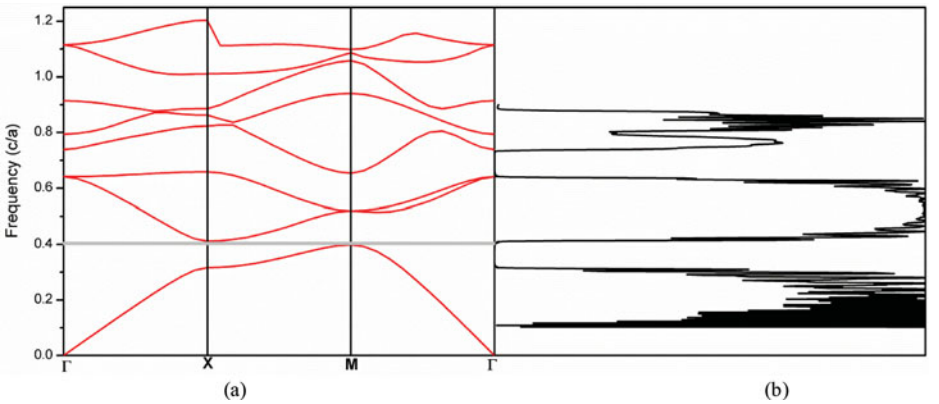

Figure 3. (a) The photonic band structure in TM mode, (b) transmission spectrum of extraordinary refractive index as a function of wavelength of core-shell-type $LiNbO_3$ round nanorods of nematic LC-infiltrated in an air background in a square lattice.

refractive index of nematic LC in a square lattice of 2D PC of core-shell-type $LiNbO_3$ round nanorods of nematic LC-infiltrated in an air background. The transmission of the extraordinary refractive index of nematic LC is zero at frequencies between $0.321(2\pi c/a)$ and $0.405(2\pi c/a)$, and between $0.647(2\pi c/a)$ and $0.732(2\pi c/a)$ (Fig. 3(b)). The transmission minima of the ordinary refractive index of nematic LC is zero at frequencies from $0.332(2\pi c/a)$ to $0.408(2\pi c/a)$ and from $0.660(2\pi c/a)$ to $0.762(2\pi c/a)$.

3.1.2. Hexagonal Lattice. Figure 4 shows the schematic views of the proposed 2D PC of $LiNbO_3$ round nanorods, core-shell-type $LiNbO_3$ round nanorods, and core-shell-type $LiNbO_3$ round nanorods of nematic LC-infill in an air background in a hexagonal lattice. In a hexagonal lattice the photonic band structure for TE and TM mode is calculated along with the high symmetry point for the Brillouin zone. Compared with the square lattice, in general the band gap is increased in a hexagonal lattice. The photonic band structure of the PC with $LiNbO_3$ round nanorods for a hexagonal lattice in an air background is simulated (Fig. 4(a)). A three band gap of TM mode is shown in Fig. 5(a) but there is no band gap in TE mode. Their relative widths are 23.47% from band 1 to band 2, 13.99% from band

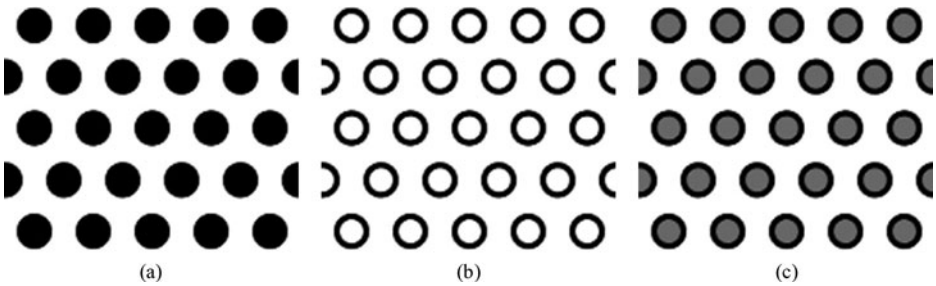

Figure 4. 2D PC structure for a hexagonal lattice (a) $LiNbO_3$ round nanorods, (b) core-shell-type $LiNbO_3$ round nanorods, and (c) core-shell-type $LiNbO_3$ round nanorods of nematic LC-infiltrated in an air background.

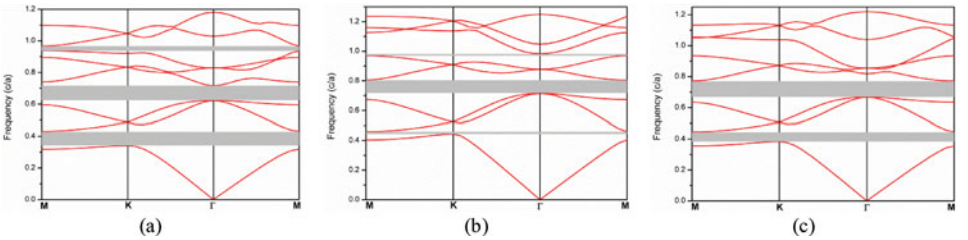

Figure 5. The photonic band structure of TM mode in a hexagonal lattice for (a) $LiNbO_3$ round nanorods, (b) core-shell-type $LiNbO_3$ round nanorods, and (c) core-shell-type $LiNbO_3$ round nanorods of nematic LC-infiltrated in an air background.

3 to band 4 and 3.03% from band 6 to band 7, and the center normalized frequencies are $0.386(2\pi c/a)$, $0.670(2\pi c/a)$, and $0.953(2\pi c/a)$.

According the PC structure as shown in Fig. 4(b), PBG become narrows in TM mode compared to $LiNbO_3$ round nanorods in a hexagonal lattice. Their relative widths are 3.57% between band 1 and band 2, 11.84% between band 3 and band 4 and 1.35% between band 5 and band 6, and the center normalized frequencies are $0.452(2\pi c/a)$, $0.760(2\pi c/a)$, and $0.977(2\pi c/a)$ (Fig. 5(b)). Comparing the square lattice with the hexagonal lattice it can be said that band gap number for TM mode is increased. PBG has one band gap in TE mode. Its relative width is 3.04% and center normalized frequency is $1.049(2\pi c/a)$.

For TE and TM mode the photonic band structure is separately analyzed for an ordinary-refractive index and extraordinary refractive index. It is seen that there is a two band gap in TM mode for both refractive indices. Figure 5(c) indicates the band gaps that have relative widths are 14.89% and 14.35%, and the center normalized frequencies are $0.415(2\pi c/a)$, and $0.720(2\pi c/a)$ for the extraordinary refractive index. The band gaps for the ordinary-refractive index have relative widths are 11.60%, 13.52%, and the center normalized frequencies are $0.426(2\pi c/a)$, and $0.733(2\pi c/a)$. Here, the presence of anisotropy was proven once again. The transmission spectrum as a function of frequency in a hexagonal lattice is similar to a square lattice. The transmission of an extraordinary refractive index of nematic LC is zero at frequencies between $0.371(2\pi c/a)$ and $0.416(2\pi c/a)$, and between $0.669(2\pi c/a)$ and $0.719(2\pi c/a)$. The transmission minima of the ordinary refractive index of nematic LC at frequencies is zero from $0.385(2\pi c/a)$ to $0.427(2\pi c/a)$ and from $0.681(2\pi c/a)$ to $0.730(2\pi c/a)$.

3.2. 2D PC of a Core-Shell-Type Ferroelectric Square Nanorod with Nematic LCs

Structure and material are very important to determine the optical properties of a PC structure as aforementioned. Therefore, we changed the PC structure in order to obtain optimum results. The materials have the same values. We consider that a 2D PC structure is composed of anisotropic nematic LCs in a core-shell-type $LiNbO_3$ square nanorod with the lattice constant $a = 1\mu m$. Parameters d_1 and d_2 denote the inner and outer length of $LiNbO_3$ square nanorods, respectively. For a square lattice and a hexagonal lattice $LiNbO_3$ square nanorods, core-shell-type $LiNbO_3$ square nanorods, and core-shell-type $LiNbO_3$ square nanorods of nematic LC-infill in an air background were designed.

3.2.1. Square Lattice. The PC structures in a square lattice for $LiNbO_3$ square nanorods, core-shell-type $LiNbO_3$ square nanorods, and core-shell-type $LiNbO_3$ square nanorods

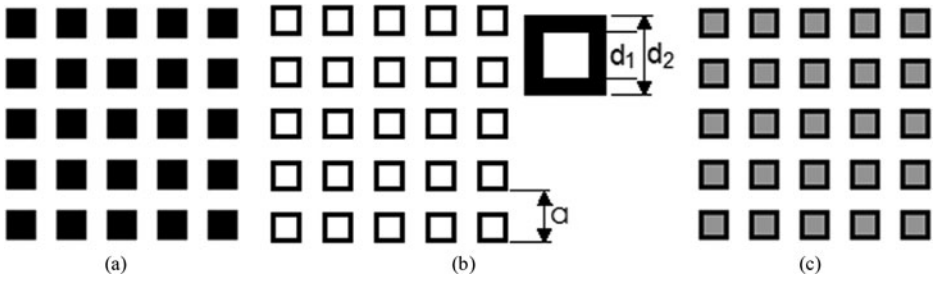

Figure 6. PC structure for a square lattice (a) $LiNbO_3$ square nanorods, (b) core-shell-type $LiNbO_3$ square nanorods, and (c) core-shell-type $LiNbO_3$ square nanorods of nematic LC-infiltrated in an air background.

of nematic LC-infiltrated in an air background are depicted in Fig. 6. It is supposed that $d_2 = 0.6a$, and the sides of the square nanorods are parallel to the primitive reciprocal lattice vectors (Fig. 6(a)). The photonic band structure for TE and TM mode is calculated along with the high symmetry point for the Brillouin zone in a square lattice. Figure 7 shows only the TM modes because there is no band gap for TE modes. According to Fig. 7(a) there is only one band gap of TM mode for $LiNbO_3$ square nanorods in a square lattice. Its relative width is 7.85% from band 1 to band 2, and the center normalized frequency is $0.354(2\pi c/a)$. When $LiNbO_3$ square nanorods are compared with $LiNbO_3$ round nanorods in a square lattice, it is seen that there is a reduction in the band gap number of the square structure.

It is supposed that $d_1 = 0.4a$ and $d_2 = 0.6a$ denotes the inner and outer length of core-shell-type $LiNbO_3$ square nanorods in an air background (Fig. 6(b)). The band diagram for this pattern is plotted in Fig. 7(b). The core-shell-type $LiNbO_3$ square nanorods have one band gap of TM mode in a square lattice. The relative width is 0.53%, and the center normalized frequency is $0.819(2\pi c/a)$. When the PC structure is turned into core-shell-type $LiNbO_3$ square nanorods, it can be clearly seen that PBG has become narrow and shifted from between band 1 and band 2 to between band 4 and band 5.

The photonic band structure of core-shell-type $LiNbO_3$ square nanorods modulated by nematic LC in TE and TM mode is again studied for ordinary-refractive index and extraordinary refractive index, individually (Fig. 6(c)). There is no band gap in TE and TM mode for both refractive indices as shown in Fig. 7(c). The transmission spectrum of the core-shell-type $LiNbO_3$ square nanorods of nematic LC-infiltrated is very close to the core-shell-type $LiNbO_3$ round nanorods of nematic LC-infiltrated in a square lattice.

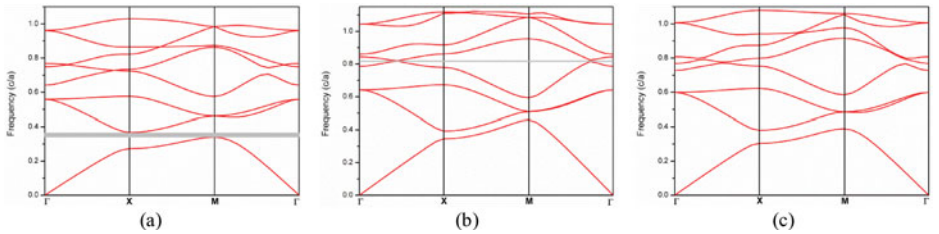

Figure 7. The photonic band structure of TM mode in a square lattice for (a) $LiNbO_3$ square nanorods, (b) core-shell-type $LiNbO_3$ square nanorods, and (c) core-shell-type $LiNbO_3$ square nanorods of nematic LC-infiltrated in an air background

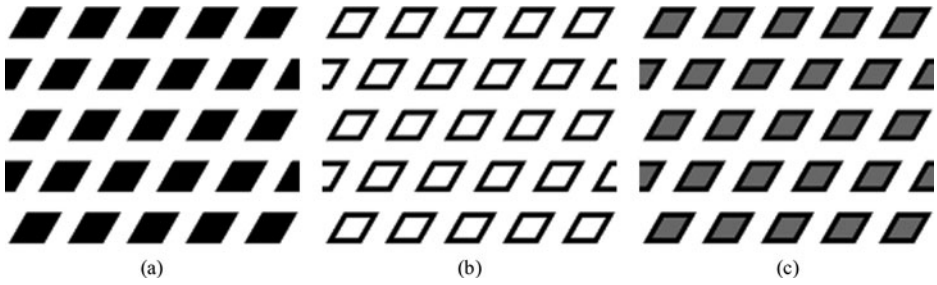

Figure 8. PC structure for a hexagonal lattice (a) $LiNbO_3$ square nanorods, (b) core-shell-type $LiNbO_3$ square nanorods, and (c) core-shell-type $LiNbO_3$ square nanorods of nematic LC-infiltrated in an air background.

The transmission of the extraordinary refractive index of nematic LC is zero at frequencies between $0.320(2\pi c/a)$ and $0.390(2\pi c/a)$, and between $0.634(2\pi c/a)$ and $0.728(2\pi c/a)$. The transmission minima of the ordinary refractive index of nematic LC at frequencies is zero from between $0.337(2\pi c/a)$ and $0.392(2\pi c/a)$, and between $0.653(2\pi c/a)$ and $0.767(2\pi c/a)$.

3.2.2. Hexagonal Lattice. For a hexagonal lattice PC structure of the offered 2D PC of $LiNbO_3$ square nanorods, core-shell-type $LiNbO_3$ square nanorods, and core-shell-type $LiNbO_3$ square nanorods of nematic LC-infilled in an air background is seen in Fig. 8. In TE and TM mode the photonic band structure is simulated along with the high symmetry point for the Brillouin zone. A three band gap TM mode as stated in Fig. 9(a) are seen for the PC structure of $LiNbO_3$ square nanorods. Their relative widths are 21.11% from band 1 to band 2, 8.76% from band 4 to band 5 and 1.94% from band 7 to band 8, and the center normalized frequencies are $0.381(2\pi c/a)$, $0.776(2\pi c/a)$ and $1.00(2\pi c/a)$. In general, the band gap number is raised in a hexagonal lattice compared with a square lattice.

The photonic band structure of the core-shell-type $LiNbO_3$ square nanorods in a hexagonal lattice becomes narrow in TM mode compared with $LiNbO_3$ square nanorods while the band gap is increased in number. Fig. 9(b) a four band gap is shown for TM mode. Their relative widths are 0.40% between band 1 and band 2, 1.29% between band 3 and band 4, 5.13% between band 4 and band 5 and 1.05% between band 7 and band 8, and the center normalized frequencies are $0.451(2\pi c/a)$, $0.756(2\pi c/a)$, $0.862(2\pi c/a)$ and $1.165(2\pi c/a)$. For TE mode one band gap occurred. The relative width is 0.81% between band 3 and band 4, and the center normalized frequency is $0.905(2\pi c/a)$.

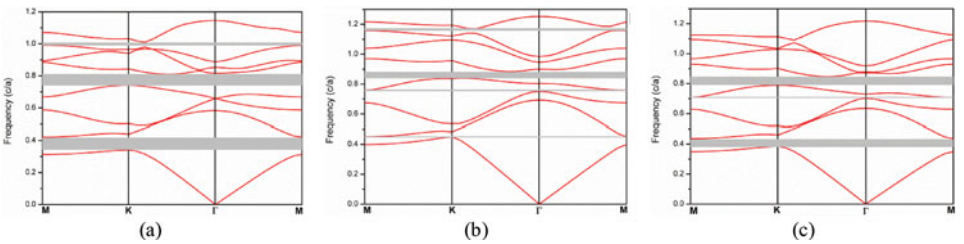

Figure 9. The photonic band structure of TM mode in a hexagonal lattice for (a) $LiNbO_3$ square nanorods, (b) core-shell-type $LiNbO_3$ square nanorods, and (c) core-shell-type $LiNbO_3$ square nanorods of nematic LC-infiltrated in an air background

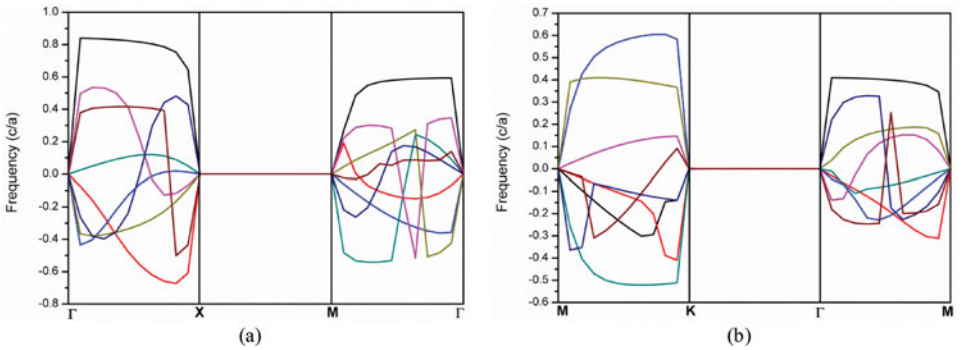

Figure 10. Group velocity for extraordinary refractive index in TE mode of core-shell-type $LiNbO_3$ round nanorods of nematic LC-infiltrated in an air background in (a) a square lattice and (b) a hexagonal lattice.

The photonic band structure of the core-shell-type $LiNbO_3$ square nanorods of nematic LC-infiltrated which has an ordinary-refractive index and extraordinary refractive index for TE and TM mode is separately examined. Although there is no band gap in TE mode, it is recorded a three band gap in TM mode for both refractive indices. Figure 9(c) specifies the band gaps that have relative widths, which are 12.31%, 0.84%, 7.11%, and the center normalized frequencies are $0.411(2\pi\,c/a)$, $0.706(2\pi\,c/a)$, and $0.818(2\pi\,c/a)$ for an extraordinary refractive index. The band gap for an ordinary-refractive index has relative widths of 8.87%, 0.85%, 6.51%, and the center normalized frequencies are $0.422(2\pi\,c/a)$, $0.721(2\pi\,c/a)$, and $0.833(2\pi\,c/a)$. When comparing square lattice with the hexagonal lattice it can be said that a three band gap for TM mode is observed. The transmission spectrum of the core-shell-type $LiNbO_3$ square nanorods of nematic LC-infiltrated is precisely similar to the core-shell-type $LiNbO_3$ round nanorods of nematic LC-infiltrated in a hexagonal lattice. The transmission of an extraordinary refractive index of nematic LC at frequencies is zero between $0.371(2\pi\,c/a)$ and $0.413(2\pi\,c/a)$, and between $0.663(2\pi\,c/a)$ and $0.703(2\pi\,c/a)$. The transmission minima of the ordinary refractive index of nematic LC at frequencies is zero from $0.389(2\pi\,c/a)$ and $0.427(2\pi\,c/a)$, and from $0.682(2\pi\,c/a)$ to $0.718(2\pi\,c/a)$.

4. Group Velocity in a Periodic Nanostructure

Assuming that $\omega n_1 A/c, \omega n_2 B/c << 1$ where ω is the radiation frequency, c is the light velocity, and A and B are the thicknesses of the alternating layers of isotropic materials with refractive indices n_1 and n_2 respectively, it can be represented that the effective refractive indices for ordinary and extraordinary waves in a periodic nanostructure are shown as [45]

$$n_0^2 = \frac{A}{D}n_1^2 + \frac{B}{D}n_2^2 \tag{8}$$

$$n_e^{-2} = \frac{A}{D}n_1^{-2} + \frac{B}{D}n_2^{-2} \tag{9}$$

where $D = A + B$. In the present paper, D is equal to the lattice constant a, A is equal to a diameter of the round nanorod or the sides of square nanorods $2r$, B is a distance between two nanorods $B = a - 2r$. n_1 is an effective refractive index of core-shell-type $LiNbO_3$ nanorods of nematic LC-infiltrated, and n_2 is an air refractive index.

Formulas (8–9) define the mixing rules for the refractive indices of the constituent materials in the case of ordinary and extraordinary waves in the periodic nanostructures. To find the corresponding mixing rules for the group velocities of light in such a nanostructure, formulas (8–9) were differentiated with respect to frequency. Generally, the group velocity for ordinary and extraordinary waves in nanostructured medium can be written as

$$\frac{1}{v_{o,e}} = \frac{g_1^{o,e}}{v_1} + \frac{g_2^{o,e}}{v_2} \tag{10}$$

where $g_i^{o,e}$ weight factor ($i = 1, 2$) depend only on the ratio B/A of layer thicknesses and the ratio n_2/n_1 of the refractive indices of the materials.

The group velocity of core-shell-type $LiNbO_3$ round nanorods of nematic LC-infiltrated in an air background in a square lattice and a hexagonal lattice for TE and TM mode is computed. Figure 10 displays the group velocity in TE mode for the extraordinary refractive index of nematic LC in a square lattice and a hexagonal lattice.

5. Conclusion

In conclusion, we have analyzed the optical properties in a 2D PC structure of a core-shell-type ferroelectric round nanorod and square nanorod infiltrated with nematic LCs in a square lattice and a hexagonal lattice. The photonic band structure for TE and TM mode is calculated along with the high symmetry point for the Brillouin zone in both of the lattices. The transmission of these PC structures as a function of wavelength is plotted. The group velocity is computed along with the high symmetry point for the Brillouin zone in the TE mode of core-shell-type $LiNbO_3$ nanorods of nematic LC-infiltrated in an air background in these lattices. We laid an emphasis on the importance of the selection of the PC structure and PC materials. As a result of this study, it was proved that the optical properties of ferroelectric materials and LCs can be controlled by an external effect such as an electric field, magnetic field, light, temperature, etc.

Acknowledgments

One of the authors (Filiz Karaomerlioglu) would like to thank The Scientific and Technological Research Council of Turkey (TUBITAK) Postdoctoral Fellowship.

Funding

This work is supported by the projects DPT-HAMIT, DPT-FOTON, and NATO-SET-193 and TUBA and TUBITAK under the Project Nos. 113E331, 109A015, and 109E301.

References

1. E. Yablonovitch, Photonic band-gap structures. *J. Opt. Soc. Am. B*. **10**, 283–295 (1993).
2. J. N. Winn, R. D. Meade, and J. D. Joannopoulos, Two-dimensional photonic band-gap materials. *J. Mod. Optics*. **41**, 257–273 (1994).
3. J. D. Joannopoulos, P. R. Villeneuve, and S. Fan, Photonic crystals: putting a new twist on light. *Nature.* **386**, 143–149 (1997).
4. T. T. Larsen, A. Bjarklev, D. S. Hermann, and J. Broeng, Optical devices based on liquid crystal photonic bandgap fibres. *Opt. Express.* **11**, 2589–2596 (2003).

5. R. Srivastava, K. B. Thapa, S. Pati, and S. P. Ojha, Desing of Photonic Band Gap Fılter. *Progress in Electromagnetics Research, PIER*. **81**, 225–235 (2008).
6. C. A. Duque and M. E. Mora-Ramos, The two-dimensional square and triangular photonic lattice under the effects of magnetic field, hydrostatic pressure, and temperature. *Opt. Quant. Electron*. **44**, 375–392 (2012).
7. B. Rezaei and M. Kalafi, Tunable full band gap in two-dimensional anisotropic photonic crystals infiltrated with liquid crystals. *Optics Commun.* **282**, 1584–1588 (2009).
8. S. W. Leonard, J. P. Mondia, H. M. Van Driel, O. Toader, S. John, K. Busch, A. Birner, U. Gösele, and V. Lehmann: Tunable two-dimensional photonic crystals using liquid-crystal infiltration. *Phys. Rev. B.* **61**, R2389–R2392 (2000).
9. C. S. Kee, H. Lim, Y. K. Ha, J. E. Kim, and H. Y. Park, Two-dimensional tunable metallic photonic crystals infiltrated with liquid crystals. *Phys. Rev. B.* **64**, 085114–085121 (2001).
10. D. M. Pustai, A. Sharkawy, S. Shi, and D. W. Prather, Tunable photonic crystal microcavities. *Appl. Opt.* **41**, 5574–5579 (2002).
11. C. Schuller, F. Klopf, J. P. Reithmaier, M. Kamp, and A. Forchel, Tunable photonic crystals fabricated in III-V semiconductor slab waveguides using infiltrated liquid crystals. *Appl. Phys. Lett.* **82**, 2767–2769 (2003).
12. C. M. Anderson and K. P. Giapis, Larger Two-Dimensional Photonic Band Gaps. *Physical Review Letters*. **77**, 2949–2952 (1996).
13. B. Maune, M. Loncar, J. Witzens, M. Hochberg, T. B. Jones, D. Psaltis, A. Scherer, and Y. Qiu, Liquid-crystal electric tuning of a photonic crystal laser. *Appl. Phys. Lett.* **85**, 360–362 (2004).
14. Z. Ma and K. Ogusu, FDTD analysis of 2D triangular-lattice photonic crystals with arbitrary-shape inclusions based on unit cell transformation. *Optics Commun.* **282**, 1322–1325 (2009).
15. Y. Y. Wang and L. W. Chen, Tunable negative refraction photonic crystals achieved by liquid crystals. *Opt. Express*. **14**, 10580–10587 (2006).
16. K. P. Chang and S. L. Yang, Photonic band gap of two-dimensional triangular photonic crystals with broken structural and rotational symmetries. *J. Appl. Phys.* **100**, 073104–073104 (2006).
17. J. A. Reyes, J. A. Reyes-Avendaño, and P. Halevi, Electrical tuning of photonic crystals infilled with liquid crystals. *Optics Commun.* **281**, 2535–2547 (2008).
18. Y. F. Chau, F. L. Wu, Z. H. Jiang, and H. Y. Li, Evolution of the complete photonic bandgap of two-dimensional photonic crystal. *Opt. Express*. **19**, 4862–4867 (2011).
19. R. P. Zaccaria, P. Verma, S. Kawaguchi, S. Shoji, and S. Kawata, Manipulating full photonic band gap in two dimensional birefringent photonic crystals. *Opt. Express*. **19**, 14812–14820 (2008).
20. N. Malkova, S. Kim, T. DiLazaro, and V. Gopalan, Symmetrical analysis of complex two-dimensional hexagonal photonic crystals. *Phys. Rev. B.* **67**, 125203–125212 (2003).
21. A. Labbani and A. Benghalia, Tunability of Photonic Band Gaps in One- and Two-dimensional Photonic Crystals Based on ZnS Particles Embedded in TiO_2 Matrix. *Photonic Sensors*. **2**, 180–186 (2012).
22. D. Liu, Y. Gao, D. Gao, and X. Han, Photonic band gaps in two-dimensional photonic crystals of core-shell-type dielectric nanorod heterostructures. *Optics Commun.* **285**, 1988–1992 (2012).
23. Z. Fan, J. Liu, S. Chen, H. Chang, C. Guan, and L. Yuan, Comparative study of photonic band gaps of germanium-based two-dimensional triangular-lattice and square-lattice and decagonal quasi-periodic photonic crystals. *Microelectronic Eng.* **96**, 11–17 (2012).
24. S. A. El-Naggar, Dependency of the photonic band gaps in two-dimensional metallic photonic crystals on the shapes and orientations of rods. *Optical Eng.* **51**, 068001–068009 (2012).
25. N. Zhu, J. Wang, C. Cheng, and X. Yan, Research of band gap properties based on two-dimensional photonic crystal with mixed shapes of rods. *Optik.* **124**, 309–312 (2013).
26. K. M. Ho, C. T. Chan, and C. M. Soukoulis, Existence of a Photonic Gap in Periodic Dielectric Structures. *Phys. Rev. Lett.* **65**, 3152–3155 (1990).
27. K. Yoshino, Y. Shimoda, Y. Kawagishi, K. Nakayama, and M. Ozaki, Temperature tuning of the stop band in transmission spectra of liquid-crystal infiltrated synthetic opal as tunable photonic crystal. *Appl. Phys. Lett.* **75**, 932–934 (1999).

28. S. G. Johnson, M. L. Povinelli, and J. D. Joannopoulos, New photonic-crystal system for integrated optics. *Proc. SPIE.* **4532**, 167–179 (2001).
29. G. Pucker, A. Mezzetti, M. Crivellari, P. Bellutti, A. Lui, N. Daldosso, and L. Pavesi, Silicon-based near-infrared tunable filters filled with positive or negative dielectric anisotropic liquid crystals. *J. Appl. Phys.* **95**, 767–769 (2004).
30. C. Y. Liu, Tunable lightwave propagation in two-dimensional hole-type photonic crystals infiltrated with nematic liquid crystal. *Physica E.* **44**, 313–316 (2011).
31. C. Y. Liu, Creation of tunable absolute bandgaps in a two-dimensional anisotropic photonic crystal modulated by a nematic liquid crystal. *Phy. Lett. A.* **372**, 5198–5202 (2008).
32. C. Y. Liu and L. W. Chen, Tunable field-sensitive polarizer using hybrid conventional waveguides and photonic crystal structures with nematic liquid crystals. *Optics Commun.* **256**, 114–122 (2005).
33. C. Y. Liu and L. W. Chen, Tunable photonic-crystal waveguide Mach-Zehnder interferometer achieved by nematic liquid-crystal phase modulation. *Opt. Express.* **12**, 2616–2624 (2004).
34. C. Y. Liu and L. W. Chen, Tunable photonic crystal waveguide coupler with nematic liquid crystals. *IEEE Photonics Tech. Lett.* **16**, 1849–1851 (2004).
35. C. Y. Liu and L. W. Chen, Tunable full bandgap in a three-dimensional photonic crystal modulated by a nematic liquid crystal. *Physica E.* **35**, 173–177 (2006).
36. C. Y. Liu and L. W. Chen, Tunable channel drop filter in a two-dimensional photonic crystal modulated by a nematic liquid crystal. *J. Nanomaterials*. **2006**, 1–6 (2006).
37. C. Y. Liu and L. W. Chen, Tunable band gap in a photonic crystal modulated by a nematic liquid crystal. *Phys. Rev. B.* **72**, 045133–045138 (2005).
38. C. Y. Liu, Y. T. Peng, J. Z. Wang, and L. W. Chen, Creation of tunable bandgaps in a three-dimensional anisotropic photonic crystal modulated by a nematic liquid crystal. *Physica B.* **388**, 124–129 (2007).
39. C. Y. Liu, N. W. Zhang, H. W. Wang, and L. W. Chen, Efficient tunable negative refraction photonic crystal achieved by an elliptic rod lattice with a nematic liquid crystal. *Physica B.* **404**, 4060–4070 (2009).
40. A. Taflove, Advances in computational electrodynamics: The Finite-Difference Time-Domain Method: A survey of The Finite-Difference Time-Domain literature. Narwood, MA: Artech House, 1–30 1998.
41. M. Plihal and A. A. Maradudin, Photonic band structure of two-dimensional systems: The triangular lattice. *Phys. Rev. B.* **44**, 8565–8568 (1991).
42. J. D. Joannopoulos, S. G. Johnson, J. N. Winn, and R. D. Meade, *Photonic Crystals: Molding the Flow of Light*. Princeton: Princeton University Press, 2008.
43. I. C. Khoo and S. T. Wu, *Optics and nonlinear optics of liquid crystals: Electro-optical properties of liquid crystals*. Singapore: World Scientific, 100–258 1993.
44. C. Kittel, *Introduction to Solid State Physics*. New York: John Wiley & Sons, 2005.
45. A. M. Zheltikov, Mixing rules for group velocities in nanocomposite materials and photonic crystals. *JETP Lett.* **79**, 57–61 (2004).